LANDSLIDE SUSCEPTIBILITY MAPPING TO INFORM LANDUSE MANAGEMENT DECISIONS IN AN ALTERED CLIMATE

By

MUHAMMAD G. BARIK

A thesis submitted in partial fulfillment of
the requirements for the degree of

MASTER OF SCIENCE IN CIVIL ENGINEERING

WASHINGTON STATE UNIVERSITY
Department of Civil and Environmental Engineering

MAY 2010

To the Faculty of Washington State University:

The members of the Committee appointed to examine the thesis of MUHAMMAD G. BARIK find it satisfactory and recommend that it be accepted.

_____

Jennifer C. Adam, Ph.D., Chair

_____

Michael E. Barber, Ph.D.

_____

Balasingam Muhunthan, Ph.D.

Acknowledgement

First of all, my sincerest gratitude goes to my advisor, Dr. Jennifer Adam, who has supported me throughout my thesis with her patience and extraordinary knowledge. She was always there to provide enough guidance and showed me different ways to approach a research problem. Without her encouragement and support this research would not have been possible. I would also like to thank Dr. Barber and Dr. Muhunthan for their valuable reviews and comments throughout the research period. My thanks go to the State of Washington Water Research Center for funding this project and providing the resources required.

I want to thank Josh for his co-operation and support from the very beginning of my research. I would like to thank Helal for his encouragement. Also, my thanks go to Kirti, Kiran, Erika, and Greg to make our office a nice place to work.

Finally, I thank my parents for supporting me throughout my studies and giving me the moral support to go for the higher studies.

LANDSLIDE SUSCEPTIBILITY MAPPING TO INFORM LANDUSE MANAGEMENT DECISIONS IN AN ALTERED CLIMATE

Abstract

By Muhammad G. Barik, M.Sc.
Washington State University
May 2010

Chair: Jennifer C. Adam

The Olympic Experimental State Forest (OESF), a commercial forest lying between the Pacific coast and the Olympic Mountains, is a region of steep slopes and high annual rainfall (2500-6000 mm/year) and is therefore highly susceptible to landslides. As this area is critical habitat for numerous organisms, including salmon, there is a need to investigate potential management plans to promote the economic viability of timber extraction while protecting the natural habitat, particularly in riparian areas. As clear-cutting reduces the root contribution, and as projected climate change may result in storms with higher intensity precipitation, this area may become more susceptible to landslide activity. This may result in potentially severe consequences to riparian habitat due to increased sediment loads. The primary objective of this study is to provide high resolution (10 m) landslide susceptibility maps over the study area to inform land management decisions in an altered climate. The Distributed Hydrology Soil Vegetation Model (DHSVM), a physically-based hydrology model with a mass wasting module,

was used to explore the sensitivity of landslide risk to timber extraction over areas with varying terrain features and soil characteristics. To investigate the impacts of climate change on landslide susceptibility we applied downscaled output from two General Circulation Models (GCMs) with two greenhouse gas (GHG) emission scenarios, A1B and B1, for the year 2045. Areas with high landslide risk increased on average 7.1% and 10.7% for the B1 and A1B GHG emissions scenarios, respectively. The maps produced in this study will enable forest managers to plan for climate change by indentifying areas that are less prone to landslide activity in an altered climate.

Table of Contents

List of Tables

List of Figures

Chapter 1: Introduction

Landslides cause significant social, economic, and environmental losses, including on average $1-5 billion of losses in several countries and around 600 deaths and thousands of injuries in total per year (Aleotti and Chowdhury 1999; Highland 2003; Blochl and Braun 2005). Although there are improvements in landslide hazard prediction, recognition, and warning systems, landslide activity is increasing worldwide (Dai et al. 2002). This increase in landslides frequency and volume may be the result of changes in climate and land use (Van Asch et al.1999).

Forest activities such as timber harvesting may increase the severity of landslide activity (Swanson and Dyrness 1975; Gresswell et al. 1979; Montgmery et al. 2000; Jakob 2000; Guthrie 2002; Brardinoni et al. 2002). These effects may be exasperated by projected changes in climate, depending on the location (Collison et al. 2000; Van Beek 2002; Schmidt and Glade 2003). By considering different landslide-controlling parameters such as topography, geography and future climate change, new forest management plans can be developed to minimize the effects of timber extraction on landslide activity. Thus, the primary objective of this study is to provide high resolution (10 m) maps of the susceptibility of landslides to timber harvesting under historical and future climate conditions. Results from this study can be used by forest managers to develop site-specific sustainable practices. The following specific questions are related to the primary objective:

1) How is landslide activity affected by timber extraction and how does this impact vary over a range of topographic, soil, and vegetation characteristics?
2) How will landslide susceptibility to timber extraction respond to projected climate change?

Chapter 2: Background

It is well known that natural events like intense rainfall, volcanic activity, and earthquakes influence landslide activity (Blochl and Braun 2005); however anthropogenic activities such as timber harvesting may also have severe consequences on slope stability, as clear-cutting in hilly forested areas may increase the frequency and volume of landslide occurrence several times compared to undisturbed forests (Swanson and Dyrness 1975; Lyons and Beschta 1983; Jakob 2000; Guthrie 2002; Dhakal and Sidle 2003). For example, the reduction of interception of precipitation by trees results in increased soil moisture and pore-water pressure because of reduced transpiration and evaporation from leaves (Simon and Collison 2002). Also, decaying roots increase the likelihood of shallow landslides by reducing reinforcement to the soil (O'Loughlin 1974; Swanson and Dyrness 1975; Burroughs and Thomas 1977; Gresswell et al. 1979; Sidle 1992; Watson et al. 1999; Roering et al. 2003).

Landslides have negative impacts on riparian ecosystems by increasing sediment loading to the streams (Brown and Krygier 1971; Beschta 1978; Ziemer et al. 1991; Brosofske et al. 1997; Lewis 1998; Smith et al. 2003; Constantine et al. 2005). This impacts fish species by reducing the success of spawning and the rearing of young salmon (Cederholm et al. 1981; Hartman et al. 1996). Timber harvesting is identified as a contributing cause for the reduction in the diversity of salmonid species in the Pacific Northwest (Reeves et al. 1993). These issues may be exasperated under future climate conditions.

Climate, particularly precipitation, plays a role in controlling landslide activity (Van Asch et al. 1999). It is anticipated that climate change will be associated with more frequent extreme climate

events such as more intense temperature differences and rainfalls events (Easterling et al. 2000) resulting in increased landslide susceptibility (Dixon and Brook 2007). To develop management practices to promote the economic and ecological sustainability of mountainous forests, the range of potential impacts of climate change on landslide susceptibility should be quantified (Spittlehouse and Stewart 2003). This is particularly true for the Pacific Northwest as this region is projected to experience both warmer and wetter winters (Mote and Salathe 2010).

The efficiency of current forest management practices to reduce harvesting-related landslide effects are not well quantified nor widely tested for long term planning (Spittlehouse and Stewart 2003). Studies have investigated the potential for best management plan's (BMPs) to minimize the impact of harvesting on landslide activities. These studies involved field data (Guthrie 2002; Brardinoni et al. 2002; Swanson and Dyrness 1975) or physically based models with distributed data and landslide inventories (Dhakal and Sidle 2003; Montgomery et al. 2000; Tang et al. 1997; Van Beek and Van Asch 2004). Most of the studies demonstrated that the recurrence interval and type of timber harvesting practices (e.g., cutting pattern, cutting frequency, and the density of remaining forest) played the greatest role in minimizing landslide activity and soil erosion (Sidle 1992; Ziemer et al. 1991; Dhakal and Sidle 2003). Most of these studies focused on the cumulative effects of harvesting and the recurrence interval of multiple timber harvests, but other geographic conditions such as soil properties and the topographic factors affecting landslide potential were considered static (Sidle 1992; Imaizumi et al. 2008) or were randomly selected (Tang et al. 1997; Dhakal and Sidle 2003). However, studies based solely on past

historical behavior showed that landslides in harvested areas are highly site specific (Brardinoni et al. 2002; Jakob 2000). Thus, most conservative harvesting techniques in high landslide susceptibility areas may not bring the optimum results of simultaneously promoting the viability of commercial timber harvesting while preserving the health of riparian areas. Identifying the most vulnerable areas to timber harvesting under current and projected future climate conditions will assist forest managers in selecting site-specific BMP's. In this study, we are meeting this need by developing the methodology to produce maps that identify the most vulnerable areas to timber extraction under various climate conditions. Incorporating the effects of climate change on landslide susceptibility maps for different harvesting scenarios is the new contribution of this study.

Chapter 3: Study Domain

Our study domain is the Olympic Experimental State Forest (OESF) of northwestern Washington, which is one of the wettest locations in the continental United States (Daly et al. 2002), with the precipitation ranging annually from 2500-6000 mm (NOAA 1978). The OESF, with a total area of 1080 km^2, is located on the western side of the Olympic Peninsula, and ranges in elevation from 0-2398 m. This area is susceptible to landslides and soil erosion because of its shallow soil, high precipitation rate, and long history of land use changes such as timber harvesting and road construction. It is managed by the Washington State Department of Natural Resource (DNR) for both timber production (which began in the early 1900's) and habitat conservation. It was brought under the current Habitat Conservation Plan (HCP) in 1997 which emphasizes improved long term forest conservation strategies based on scientific research and studies (DNR 2007). As an experimental forest, the OESF has a unique approach to integrate production and conservation under un-zoned forest management. The Hoh, Bogachiel, Calawah, Hoko, Sol-e-Duc, and Queets are some of the river basins in this area. For this study the Queets Basin (Figure 3.1) was selected because it has wide range of geographical properties (e.g. steep slopes and high elevation) with a long period of recorded historical streamflow data (1948-present) and an inventory of landslides. The upper basin lies in the Olympic National Park and the National Forest while the lower basin is managed by the DNR where wide spread logging has occurred.

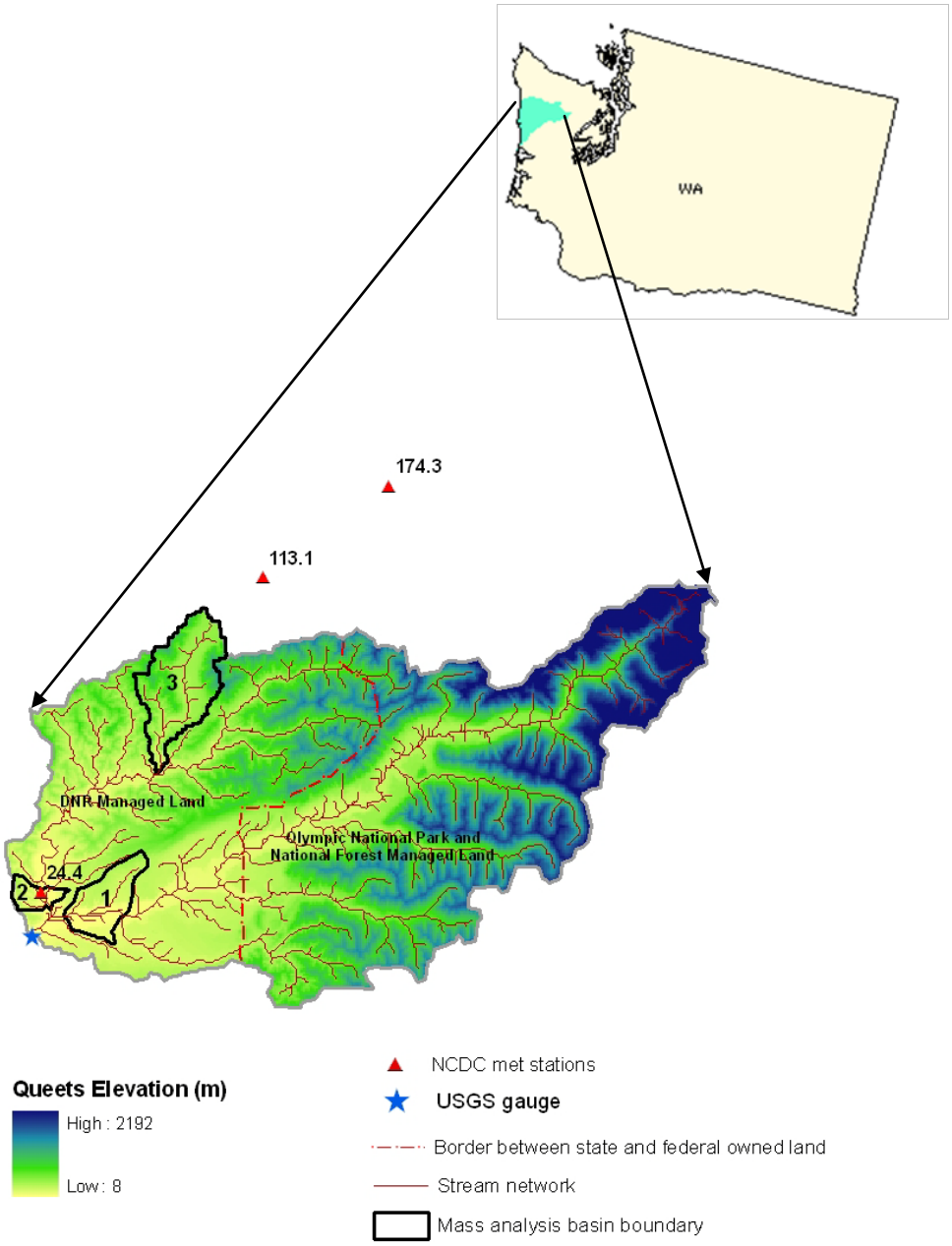

Figure 3.1 The Queets Basin, located on the Olympic Peninsula of Washington State. While we simulated the hydrologic processes over the entire basin, the mass wasting (landslide) analysis was applied only for sub- basins 1, 2 and 3. National Climatic Data Center (NCDC) weather stations are shown as red triangles with their elevations (m) shown as black text.

Chapter 4: Data and Methods

4.1. Model

We applied the Distributed Hydrology Soil Vegetation Model (DHSVM; version 3 r2) (Wigmosta et al. 1994), which is a fully-distributed physically-based hydrology model with a sediment module (Doten et al. 2006). This model was selected because of its numerous applications in the mountainous regions of the Pacific Northwest (e.g. Wigmosta et al. 1994; Wigmosta and Lettenmaier 1999; Doten et al. 2006; Alila and Beckers 2001). DHSVM has a single layer energy balance model for snow melt intercepted by canopy and a two layer energy-balance model for snow accumulation and melt on the ground. Vegetation in this model is represented by a two layer canopy model with two layers of rooting zones. Darcy's law is applied to simulate unsaturated soil moisture movement and a quasi three dimensional model is used to determine saturated sub-surface flow (Wigmosta and Lettenmaier 1999). Overland flow occurs when the precipitation rate surpasses the maximum infiltration rate. The mass wasting module, which is one of the four primary components of the DHSVM sediment module (see Figure 4.1), was used for predicting landslides. This algorithm is suitable for shallow landslide prediction (Doten et al. 2006) which is frequent in the study area (Slaughter and Lingley 2006). Failure prediction in each grid cell of this model is based on the infinite slope stability method. For a cell to fail, the factor of safety (FS) must be less than one, which is determined by root cohesion, soil cohesion, soil angle of internal friction, terrain slope, saturated fraction of total soil depth, vegetative surcharge, and the unit weight of soil (Doten et al. 2006).

The DHSVM mass wasting module is stochastic in nature in that it calculates the FS (equation 1) based on user-defined probabilistic distributions of soil cohesion, angle of internal friction, root cohesion, and vegetation surcharge. A normal distribution is used for the vegetation parameters (root cohesion and surcharge). For soil parameters both normal and uniform distributions are used. This module runs for only probable mass wasting dates. These seven storm events (one for each year) between 1984 and 1990 were selected as the events that produced the highest saturation extent in the basin.

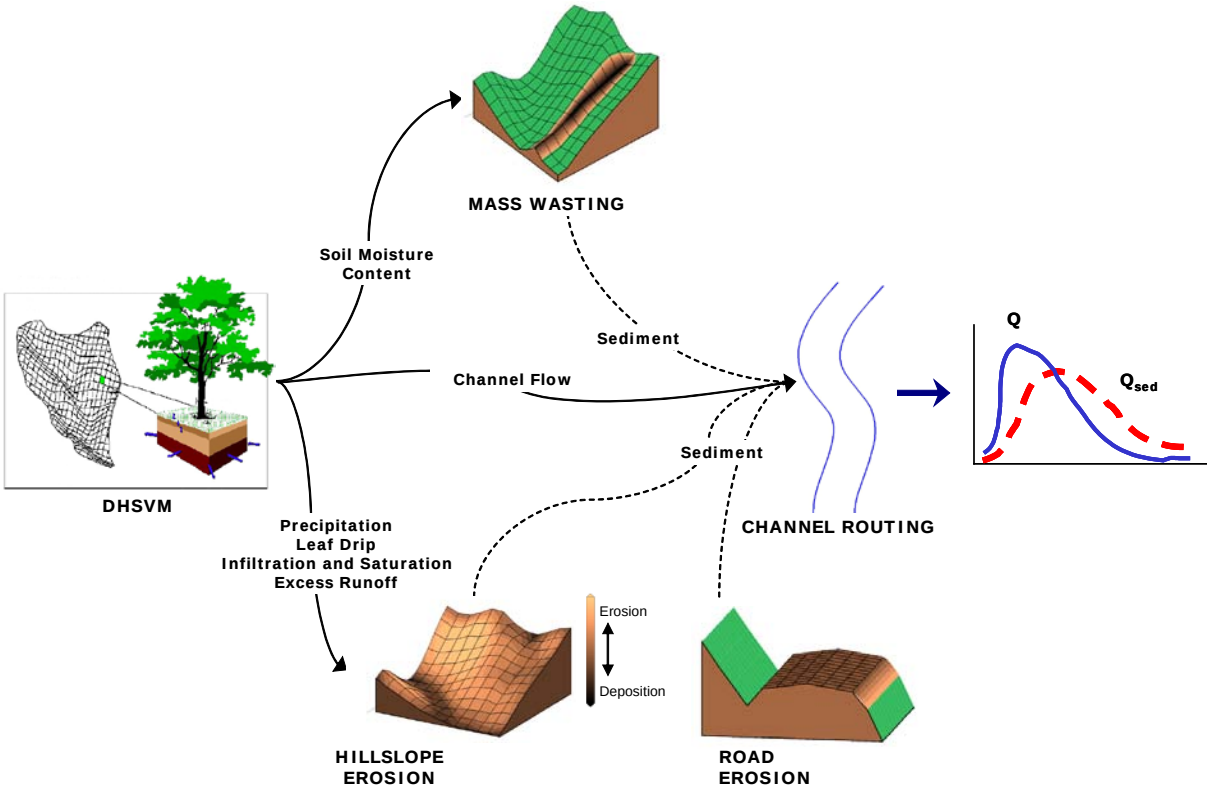

Figure 4.1 The DHSVM sediment module with its four components (used with the permission of the authors; Doten et al. 2006). This study applies the mass wasting components of the sediment module.

The FS calculation of the model is based on the following equation:

$$\mathbf{FS}=\frac{\left(\frac{2(Cs+Cr)}{\gamma_w d \sin(2S)}+\frac{(L-m)\tan\emptyset}{\tan(S)}\right)}{L}, \qquad \mathbf{(1)}$$

where,

$$\mathbf{L}=\frac{q_0}{\gamma_w d}+ m \frac{\gamma_{sat}}{\gamma_w}+ (1-m)\frac{\gamma_m}{\gamma_w},$$

C_S = Soil cohesion, C_r = Root cohesion, Φ= Angle of internal friction, d= Depth of soil, m= Saturated depth of soil, S = Surface slope, q_0 = Vegetation surcharge, γ_w = Unit weight of water, γ_{sat} = Saturated unit weight of soil, and γ_m = Unit weight of soil. DHSVM landslide prediction is most sensitive to soil cohesion, root cohesion, and the depth of soil (Doten et al. 2006).

4.2. Data

The Digital Elevation Model (DEM) source was the Shuttle Radar Topography Mission (SRTM 2000) 1 arc-second resolution elevation dataset (U.S. Geological Survey 2000). The DEM was re-sampled to the coarser resolution of 150 m for hydrologic simulation. A high resolution DEM was required for the mass wasting module, and we applied a 10 m DEM that was developed by the University of Washington Geomorphological Research Group (UWESS 2001). This DEM was created from USGS topographic maps with a 40 ft contour interval (U.S. Geological Survey 1992). The 150 m DEM was used to classify elevation (Figure 4.2a) and the 10 m DEM was

used to classify slope (Figure 4.2d).

The Queets Basin boundary was delineated in ArcINFO© using the 150 m DEM which resulted in a contributing area of 1153 km^2 (Figure3.1). The stream network was verified against a Washington State published atlas (Washington Atlas and Gazetteer 1998).

The soil classification (Figure 4.2b) was obtained by University of Washington researchers (under the Hood Cannel Project; HCDOP 2005), who reclassified Washington State DNR (WADNR 2003) soil survey data into 18 soil texture classes using the soil texture triangle developed by the U.S. Department of Agriculture (Soil Conservation Service 1975). The soil hydraulic properties, such as hydraulic conductivity, porosity, maximum infiltration, and pore size distribution, were obtained from Maidment (1992) and Chow et al. (1988). The soil depth grid file was based on the cumulative drainage area and slope. Three important soil parameters (soil cohesion, angle of internal friction, and porosity) for the mass wasting module were obtained from Lindeburg (2001), Koloski et al. (1989), and Maidment (1992) and are listed in Table 4.1. The maximum soil depth was taken as 2 m, as shallow landslides that occur in the Pacific Northwest are limited to this depth (Schmidt et al. 2001; Doten et al. 2006).

Table 4.1 Soil parameters needed for the mass wasting module: soil cohesion, angle of internal friction (Lindeburg 2001; Koloski et al. 1989), and porosity (Maidment 1992). Both the maximum and minimum values of the angle of internal friction were used to obtain a normal distribution.

Soil Types	Soil Cohesion (kPa)	Angle of Internal friction (min)	Angle of Internal friction (max)	Porosity
Sand	0	30	35	0.43
Silty Loam	21	30	40	0.48
Loam	23	30	40	0.43
Silty Clay Loam	15	15	30	0.43
Clay	13.5	20	30	0.38
Talus	0	45	45	0.1

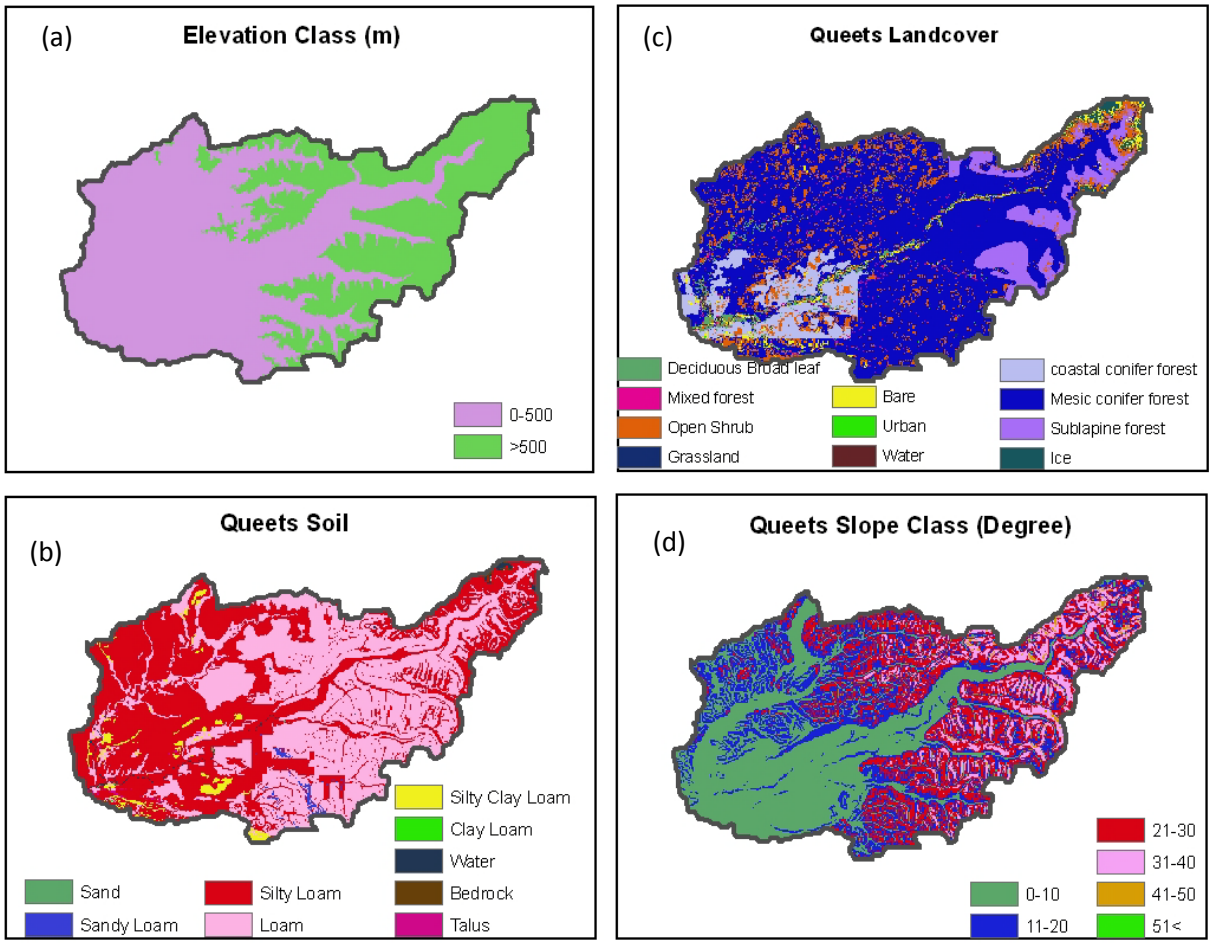

Figure 4.2 (a) Elevation (USGS 2000), (b) soil type (HDCOP 2005), (c) land cover (NOAA 1990) and (d) slope (UWESS 2001) in the Queets Basin.

The land cover data (Figure 4.2c) were derived from NOAA's Coastal Change Analysis Program (NOAA 1990) which used year 2001 Landsat-TM imagery (NASA 1999). The data were re-sampled from 30 to 150 m for application over the Queets Basin. This dataset has 29 land cover classes, 11 of which are present in the OESF.

4.3. Meteorological Data

Daily climate inputs required by DHSVM are minimum and maximum temperature, precipitation, incoming shortwave and incoming longwave radiation, surface humidity, and wind speed. The precipitation and temperature data used in this study were developed by Deems and Hamlet (2010), who extended (1915-2006) and improved ($1/16^{th}$ ° resolution, temperature rescaling) the Maurer et al. (2002) gridded data. NCEP/NCAR Reanalysis wind speed data (Kalnay et al. 1996) were used as daily wind data. Relative humidity, shortwave radiation and longwave radiation were calculated from temperature and precipitation data using methods described by Maurer et al. (2002). These $1/16^{th}$ ° historical meteorological data were developed as forcing data for the Variation Infiltration Capacity (VIC) model (Elsner et al. 2010) and customized to the DHSVM-compatible time-step of 3-hours.

4.4. Landslide Inventory

We applied the Washington State DNR digital landslide database (1900-2000), which was developed under the Landslide Hazard Zonation Project (DNR 2009). Although the landslides were identified via aerial imagery, 15-20% of the landslides were confirmed by field visit (Slaughter and Lingley 2006). Using a Geographical Information System (GIS), we calculated projected areas of these mass wasting events to compare with model simulated results. Because of the stochastic nature of DHSVM, the exact locations of simulated and observed landslides are not comparable; thus only area-wide statistics were calculated and compared. Deep-seated landslides can also occur in this region but were not included in our comparisons as the model

only simulates shallow landslides. Deep-seated landslides were separated from shallow landslides using the landslide-category information in the DNR landslide inventory. However, this information was not available for all of the landslides in the database. Thus, slides greater than 10,000 m^2 in surface area were considered as deep-seated as very few shallow landslides greater than this extent have been observed in the Pacific Northwest (Montgomery et al. 1998).

4.5. Timber Harvest Identification

We applied Landsat 5-TM (NASA 1984) images to identify historical deforestation activities. Multiple studies across the globe have confirmed that Landsat images can detect timber harvesting with high confidence using a variety of methods (Sader and Winne 1992; Skole and Tucker 1993; Cohen et al. 1998; Wilson and Sader 2002; Sohn and Rebello 2002). For this study we used the supervised classification method as applied by Sohn and Rebello (2002).

Landsat-5 TM images used for this study were collected from the USGS Global Visualization Viewer (GLOVIS 2006). Images with the least amount of cloud cover (August 1986, September 1990 and August 1996) were selected and processed using ENVI©. We applied the Chander and Markham (2003) radiometric calibration procedures for converting the digital numbers (DN's) from image data to top-of-atmospheric reflectance. Following the method outlined by Sohn and Rebello (2002), the area was classified into five types of landcover: clear-cut, old growth trees, newly planted trees or grassland, developed areas, and water. Three control points of known vegetation for each land cover type were used to train the classification. We selected these

control points from a 1990 USGS National Aerial Photography Program (NAPP) image (U.S. Geological Survey 1991). We applied a sequential image differencing approach (Cohen et al. 1998) to reduce the error in miss-classifying naturally bare or non-forested lands as clear-cut. For this, we also processed Landsat images for 1986 and 1996 (before and after our 1990 image). Any areas classified as clear-cut in all three images were re-labeled as permanent bare land (because the areas would have been replanted in the meantime if they had experienced clear-cutting). Figure 4.3 shows the results of the supervised classification methodology over a portion of the study area.

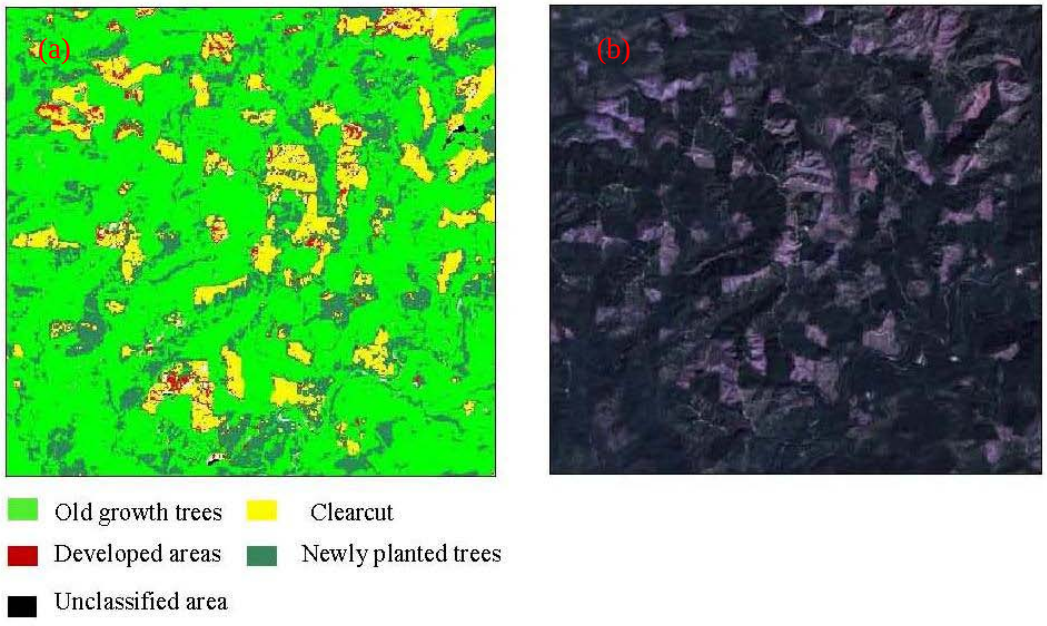

Figure 4.3 (a) Land cover classification results using the supervised classification method of Sohn and Rebello (2002). (b) The raw landsat-5 TM image of September 1990.

4.6. Susceptibility Mapping

Landslide susceptibility mapping methods can be classified according to whether they are distributed, qualitative, statistical, deterministic, or hybrid techniques (Mantovani et al. 1996; Saha et al. 2005; Ayalew et al. 2005). All of these techniques are based on the relationships of different landslide controlling factors with landslides observations (Guzzetti et al. 1999; Lee and Min 2001). Landslide susceptibility mapping by the quantitative statistical analysis method (Ayalew et al. 2005; Saha et al. 2005) is a very popular and widespread technique that applies historical landslide data to relate landslide susceptibility to multiple landslide controlling factors (e.g., slope and soil properties) (Anbalagan 1992; Dhakal et al. 1999; Remondo et al. 2008). The Landslide Susceptibility Index (LSI) reflects past slope behavior in a region and is used as an indicator of potential landslide activity (Wang and Sassa 2005) but does not incorporate the potential influence that climate change may have on slope stability. We applied a bivariate statistical method which was first developed by Yin and Yan (1988), later simplified by Van Westen (1997), and applied by Saha et al. (2005). Van Westen (1999) calculated a set of weights for a particular landslide controlling factor (e.g., slope; see list of factors in Table 4.2) according to the following equation:

$$W_i = ln\frac{(Densclas)}{(Densmap)} = \ln\left(\frac{\frac{Npix(Fi)}{Npix(Ni)}}{\frac{\sum_{i=1}^{n} Npix(Fi)}{\sum_{i=1}^{n} Npix(Ni)}}\right) \quad \text{for all i,} \qquad (2)$$

in which, Wi = the weight given to a certain class, i (e.g., 11-20°; see list of classes for each factor in Table 2); Densclas = the landslide density within the class, i; Densmap = the landslide

density within the entire map (for that factor); Npix(Fi) = number of pixels, which contain landslides, in a certain class; and Npix(Ni) = total number of pixels in a certain class.

Weights calculated by this logarithmic equation give negative values when landslide susceptibility is low and positive values when it is high within a certain class. Use of the logarithmic function form in equation 2 can be explained by Mogami (1977). After calculating the weight, W_i, for each class within each factor, the landslide susceptibility map was created by summing the weights over each pixel.

Table 4.2 Elevation, slope, soil, and vegetation classes used for the landslide susceptibility mapping.

Factor	Class
Elevation (m)	0-500 >500
Slope (°)	11-20 21-30 31-40 41-50 >50
Soil Texture	Sand Silty Loam Loam Silty Clay Loam Clay Talus
Land Cover	Deciduous Broadleaf Coastal Conifer Mesic Conifer Deciduous Broadleaf

4.7. Model Scenarios

4.7.1. Climate Change Scenarios

For regional or basin-scale climate change studies, downscaled climate data generated from Global Circulation Models (GCMs) are required. GCM selection is a critical process, especially for studies involving shallow landslides which are usually rainfall induced (Buma and Dehn 1998; Dixon and Brook 2007). We selected CGCM_3.1t47 (Kim et al. 2002) and CNRM-CM3 (Salas-Mélia et al. 2006) as they have resulted in the least amount of precipitation bias when compared with observed climate data (Mote and Salathe 2010). We have considered precipitation because of its association with landslides. We applied the Elsner et al. (2010) downscaled precipitation and temperature output from these GCMs. Elsner et al. (2010) downscaled the GCM output to $1/16^{th}$ ° over the Pacific Northwest using a newly developed hybrid method (Hamlet et al. 2010) that combines the quantile-based bias correction methodology (see Wood et al. 2002 and Wood et al. 2004 for details) with the non-transient delta change method (Loáiciga 2000). The 2045 monthly precipitation and temperature changes were used to perturb the 30-year observed climate record (1970-2000). The IPCC GHG emissions scenarios A1B and B1 were selected, as they are high and low scenarios, respectively (Nakicenovic and Swart 2000).

4.7.2. Harvesting scenarios

Logging scenarios were selected based on different slope, elevation, soil, and vegetation classes as detailed in Table 4.2. Clear-cutting was simulated by changing root cohesion, tree surcharge, and the tree rainfall interception fraction. We have used published values for root cohesion

(summarized in Table 4.3). While simulating clear-cut, we considered the worst possible reduction in root cohesion or vegetation surcharge for all harvesting scenarios to represent the most vulnerable condition under different storm events. Clear-cutting can reduce root cohesion to 2.5-0.5 kPa (Sidle 1992). For this study, post-logging root cohesion values were collected from Sidle (1992) (Table 4.3). Vegetation surcharge does not have a significant effect on slope stability as compared to the weight of soil above the failure plane (Wu and Sidle 1995; Sidle 1992). Thus, we applied a constant value of 255 kg/m^2 of vegetation surcharge from a study for deciduous broadleaf, coastal conifer, and mesic coniferous forest types (O'Loughlin 1974) and a reduced value of 150 kg/m^2 for un-matured mixed forest types. This vegetation surcharge was reduced to zero for post-logging scenarios.

Table 4.3 Root cohesion in pre and and post-harvesting conditions.

Forest Type	Maximum Root Cohesion (kPa)	Post Logging Root Cohesion (kPa)	References
Deciduous Broadleaf	7	0.5	Schmidt et al. 2001
Coastal Conifer	22	2.5	Sidle 1991
Mesic Conifer	17.5	2.0	Schmidt et al. 2001
Mixed (Not Matured)	6	0.5	Sidle 1991

Chapter 5: Results and Discussion

5.1. Evaluation of Hydrologic Modeling Results over the Queets Basin

The DHSVM implementation over the Queets Basin was calibrated and evaluated with historical USGS streamflow measurements at the outlet of the Queets Basin (recall Figure 3.1). DHSVM-simulated streamflow is sensitive to several soil parameters, including lateral hydraulic conductivity, vertical hydraulic conductivity, maximum infiltration rate, and porosity. These parameters were therefore targeted for calibration and values were chosen to reduce the error in simulated streamflow. The streamflow record was divided into the calibration and evaluation periods of 1991-1995 and 1985-1990, respectively. The Nash Sutcliffe efficiency (Nash and Sutcliffe 1970) for streamflow was 0.74 and 0.71 over the calibration and evaluation periods, respectively; while the relative bias for annually-averaged streamflow was -13% and -8% for the calibration and evaluation periods, respectively. The relative bias is simulated minus observed flows as percentage of observed flow. Comparison of monthly simulated and observed streamflow demonstrates that, while the timing of the peaks is good, we are underestimating the magnitude of the peaks (Figure 5.1), which we believe to be caused by an underestimation of precipitation. Although the precipitation data used to drive the model have been adjusted to account for orographic influences using the Parameter-elevation Regressions on Independent Slopes Model (PRISM; Daly et al. 2002), we suspect that the data do not capture the strong gradients of precipitation with elevation that are known to occur on the western slope of the Olympic Peninsula (Minder et al. 2008). As the precipitation gauges are located in the lower

elevations (Figure 3.1), it is probable that the under-prediction of streamflow is due to underestimated precipitation over the higher elevations. Because we are investigating the effects of timber harvest on landslide activity, we are primarily interested in landslide susceptibility over the lower half of the Queets Basin which is in DNR lands and subject to logging. Therefore, to the extent that is suggested by Figure 5.1, we may not be underestimating precipitation in the lower basin where we focus our landslide study. Furthermore, Figure 5.2 and Table 5.1 demonstrate that the relative bias is smallest during the winter, the period during which most landslide activity in this region occurs (Minder et al. 2009).

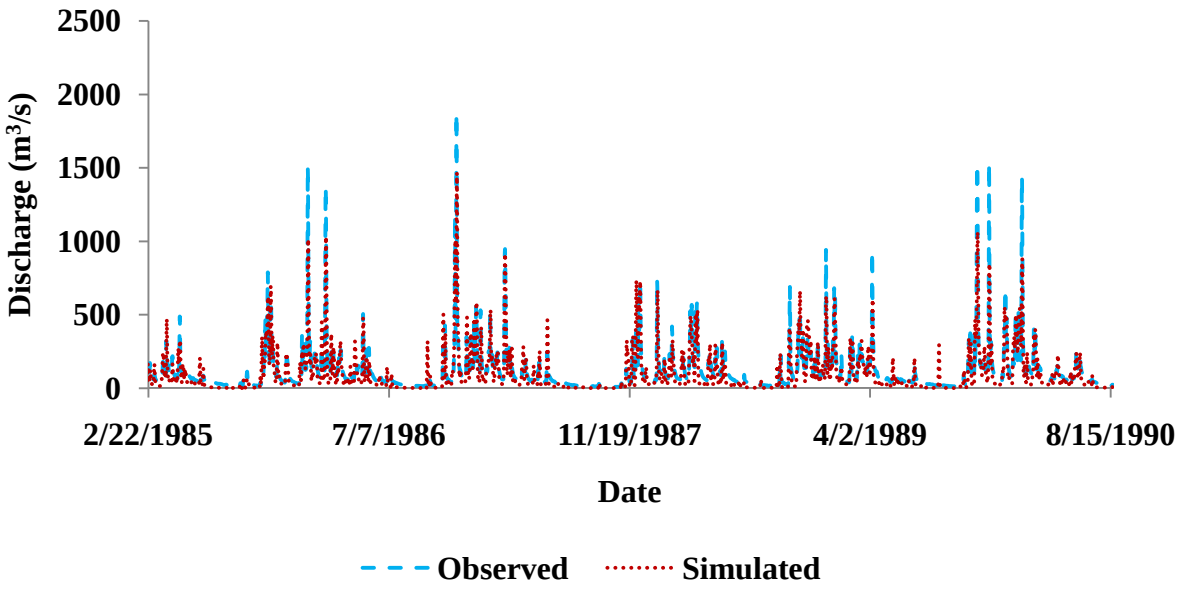

Figure 5.1 Observed and modeled streamflow over the evaluation period of 1985-1990, for which the Nash Sutcliffe efficiencies and relative biases are 0.71 and -13%, respectively.

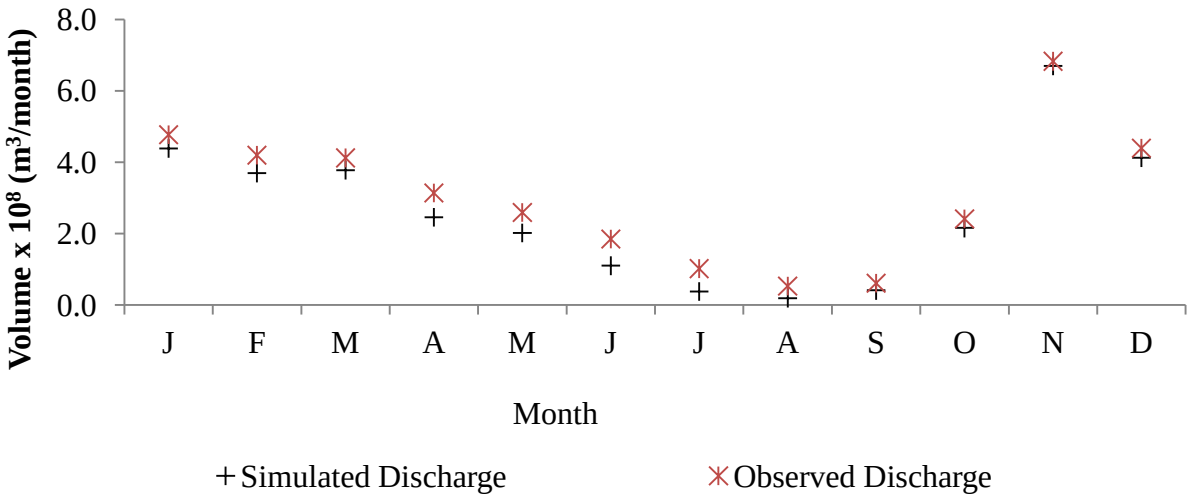

Figure 5.2 Monthly average observed and simulated streamflow over the evaluation period of 1985-1990.

Table 5.1 Monthly relative bias, calculated during the evaluation period of 1985-1990.

Month	Observed Discharge x 10^8 (m^3/month)	Simulated Discharge x 10^8 (m^3/month)	Relative Bias (%)
Jan	4.77	4.39	-8.0
Feb	4.20	3.70	-11.9
Mar	4.12	3.78	-8.4
Apr	3.14	2.46	-21.7
May	2.59	2.02	-22.1
Jun	1.85	1.10	-40.4
Jul	1.02	0.38	-62.5
Aug	0.53	0.19	-63.9
Sep	0.61	0.41	-32.8
Oct	2.42	2.16	-10.6
Nov	6.83	6.70	-1.9
Dec	4.39	4.13	-6.1

5.2. Evaluation of the DHSVM Mass Wasting Model over Sub-Basins of the Queets

Three sub-basins (shown in Figure 3.1) from the Queets were selected for application of the DHSVM mass wasting module as this process is time-consuming and computationally-intensive. Sub-basins 1 and 2 were selected to evaluate for the mass wasting results, and 1 and 3 were selected for the timber harvesting analysis. The largest storm events during 1985 and 1981 were selected to evaluate the mass wasting model over sub-basins 1 and 2, respectively; the results of which are given in Table 5.2. The relative biases between predicted and historical landslide area are 7.4% and -10.4% for sub-basins 1 and 2, respectively. However, there may be biases (that we are not able to quantify) in the landslide inventory itself that may originate from errors in interpreting the aerial photography.

Table 5.2 Mass wasting module evaluation results. Both observed and simulated landslide surface areas were greater for sub-basin 2 than for sub-basin 1.

Sub-basin	Slide year	Total Surface Area of Observed Landslides (m^2)	Total Surface Area of Simulated Landslides (m^2)
1	1985	10614	11400
2	1981	15257	13678

5.3. Landslide Susceptibility Mapping

5.3.1. Weights for Each Landslide-Controlling Factor

Firstly, both sub-basins were run for the base case (before timber extraction) scenario which resulted in simulated failure areas of 0.0004% and 0.008% for sub-basins 1 and 3, respectively. Secondly, the model was run for all of the harvesting scenarios. The landslide activity in the baseline scenario was subtracted from the landslide activity in each of the harvesting scenarios to isolate the failure events that were influenced by logging activities. The simulated failures in different harvesting classes were used to calculate the weights according to equation 2 (section 4.6). To calculate these weights, we ran the DHSVM mass wasting module for the largest storm events occurring in each of the seven years between 1984 and 1990. Table 5.3 represents the weights for each class of each landslide-controlling factor.

5.3.2. Susceptibility Classes

To compare these weights against historical landslide activity, we selected an area near the mouth of the Queets Basin that has experienced logging-related landslides (Figure 5.3). A spatial distribution of logged areas was determined from a 1990 Landsat TM image using the supervised classification method as described in section 4.5. The observed landslides between the period of 1990-1997 were identified using the DNR HZP inventory (DNR 2009) and shown in Figure 5.3.

The Saha et al. (2005) probability distribution approach was used to determine the susceptibility classes. The susceptibility map was created for the harvested areas in that region by summing the

appropriate weights from Table 5.3 for each pixel (also shown in Figure 5.3). Over harvested areas, the range of susceptibility values was -3.24 to 2.21, and was divided into three susceptibility classes using thresholds of 33% and 67% of the cumulative susceptibility. As shown in Table 5.4, these thresholds were assigned to susceptibility values of 0.05 and 0.79, respectively, resulting in three susceptibility classes: low (<0.05), medium (0.06 to 0.79), and high (>0.79). Frequencies of historical landslides for each of the susceptibility classes were calculated and we found that higher susceptibility classes are associated with higher frequency values (Table 5.4), demonstrating that the susceptibility classes roughly capture the general relationships between the landslide-controlling factors and landslide activity.

Table 5.3 Weights calculated using equation (1) for historical and climate change scenarios. Section A shows the total number of landslides under different climate change and harvesting scenarios. Section B shows only the logging-related landslides, which were determined by subtracting the landslide activity in the harvesting scenarios from the landslide activity in the baseline (no harvesting) scenario. US*: Slopes less than 10° are unconditionally stable; as the model does not consider FS calculations up to 10° slope (see Doten et al. 2006), weights were not calculated in this slope range.

		(A)Total basin landslides					(B)Harvesting-related landslides					(C)Weight				
Classes	Total Area	Historical Climate	CGCM A1B	CGCM B1	CNRM A1B	CNRM B1	Historical Climate	CGCM A1B	CGCM B1	CNRM A1B	CNRM B1	Historical Climate	CGCM A1B	CGCM B1	CNRM A1B	CNRM B1
(a)Elevation (m)																
0-500	703575	45816	46790	46599	46781	46895	41636	42610	42420	42601	42715	-0.06	-0.04	-0.04	-0.04	-0.03
>500	39375	9220	9553	9393	9269	9544	5040	5374	5213	5089	5364	0.71	0.78	0.75	0.72	0.77
(b)Slope (°)																
<10	US*	US*	US*	US*	US*	US*	US*	US*	US*	US*	US*	US*	US*	US*	US*	US*
10-20	225900	27370	29339	29023	29237	29386	23191	25160	24844	25057	25207	0.60	0.68	0.67	0.68	0.68
20-30	95625	17554	18381	18778	18983	18361	13375	14202	14598	14803	14182	0.91	0.97	1.00	1.01	0.97
30-40	11475	6389	6439	6500	6453	6450	2210	2260	2320	2274	2270	1.23	1.25	1.28	1.26	1.26
40-50	6750	1548	1562	1563	1556	1584	1447	1461	1462	1455	1483	1.34	1.35	1.35	1.34	1.36
>50	8550	1695	1697	1696	1697	1698	1594	1596	1595	1596	1597	1.20	1.20	1.20	1.20	1.20
(c)Soil																
Sand	1350	231	247	253	242	256	130	146	152	141	155	0.47	0.59	0.63	0.56	0.65
Silty Loam	549450	40271	40717	40788	40801	41024	36091	36538	36608	36622	36844	0.09	0.10	0.11	0.11	0.11
Loam	159300	10959	11258	11148	11086	11179	6780	7079	6968	6907	6999	-0.34	-0.30	-0.31	-0.32	-0.31
Silty clay Loam	25425	5172	5248	5261	5231	5248	992	1068	1081	1052	1068	-0.43	-0.35	-0.34	-0.37	-0.35
Clay	4950	129	130	132	133	132	28	29	31	32	31	-2.38	-2.34	-2.27	-2.24	-2.27
Talus	2475	4654	4698	4711	4707	4695	475	518	532	528	515	1.16	1.25	1.28	1.27	1.25
(d) Vegetation																
Deciduous Broadleaf	31950	4924	5005	5017	5005	5008	745	825	838	826	828	-1.29	-1.18	-1.17	-1.18	-1.18
Mixed forest	8100	4967	4978	5007	5044	5005	787	798	827	864	825	0.14	0.15	0.19	0.23	0.19
Coastal conifer forest	37575	1269	1272	1276	1272	1275	1168	1171	1175	1171	1174	-1.00	-1.00	-0.99	-1.00	-0.99
Mesic conifer forest	464400	34616	36186	36579	36165	36661	30436	32007	32399	31986	32482	-0.25	-0.20	-0.19	-0.20	-0.19

Table 5.4 Frequency of observed landslides in each of the model-derived susceptibility classes. The frequency of observed landslides increases with higher simulated landslide susceptibility.

Susceptibility Class Segmentation	No. of actual landslide cells in each susceptibility class	No. of total cells in each susceptibility class	Percentage of actual landslides in each susceptibility class
Low (<0.05)	621	28049	2.2%
Medium (0.05-0.79)	617	25099	2.5%
High (>0.79)	627	19021	3.3%

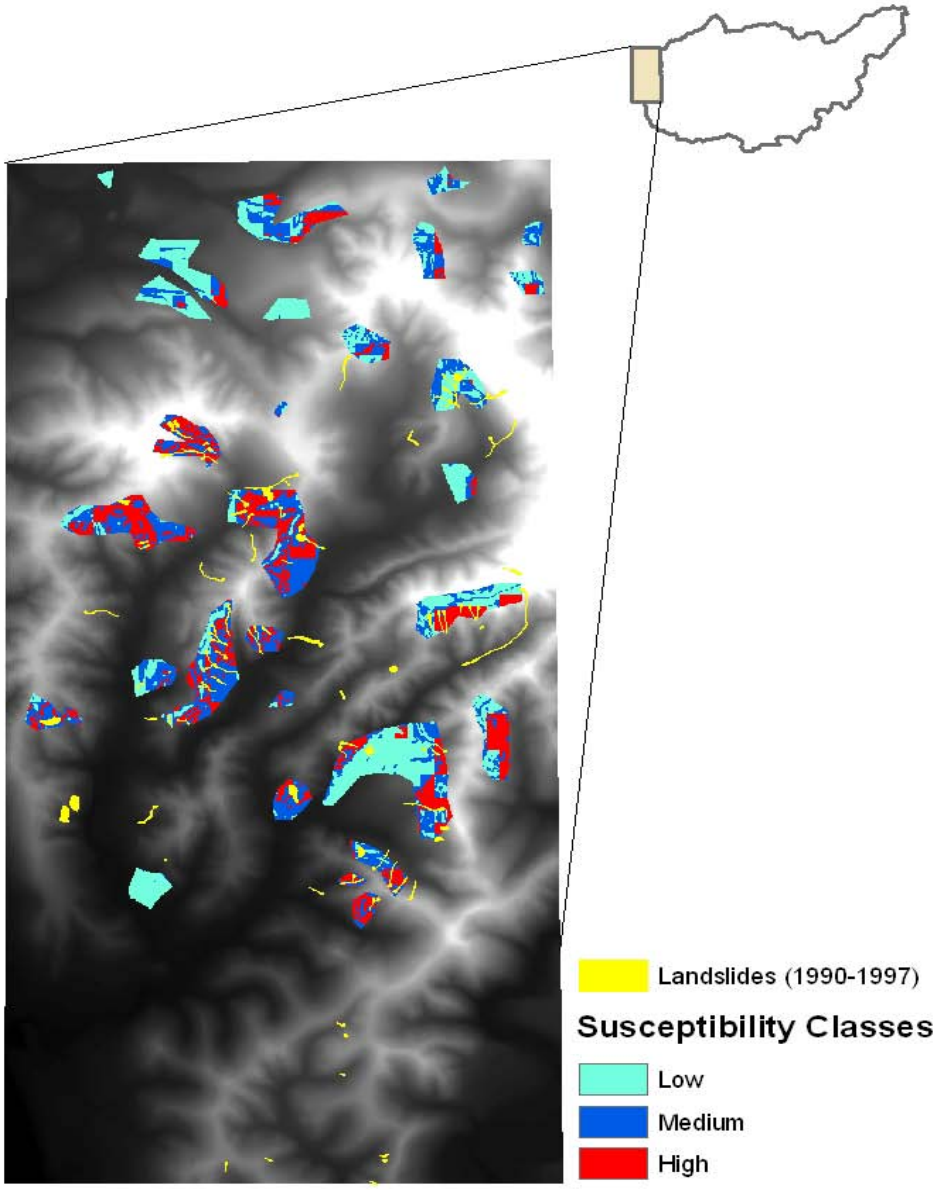

Figure 5.3 Area selected for comparison of the simulated landslide susceptibility classes to observed landslide activity. The yellow areas identify the locations of historical landslides (DNR 2009) between 1990 and 1997. All of the polygons are historically-logged areas as detected by Landsat5 imagery. Within these logged areas are the three simulated landslide susceptibility classes (see text for details).

5.4. Impacts of Timber Harvesting

We have developed a model-based strategy to map logging-induced landslide susceptibility, which can provide a useful tool to forest managers in developing site-specific management plans. However, this method does not help us understand the individual controls that each of the landslide-controlling factors have on logging-induced landslide activity because the method does not isolate these controls. Therefore, to investigate individual contributions of different factors, we have analyzed the post-harvesting sensitivity of landslide activity to different slope, soil and vegetation classes.

The incidence of logging-induced landslides for the historical climate scenario was plotted against each slope class (Figure 5.4). As expected, the model showed that slope has strong controlling effect on landslide activity. The highest slope class has more than twice the logging-induced landslide activity than the lowest slope class.

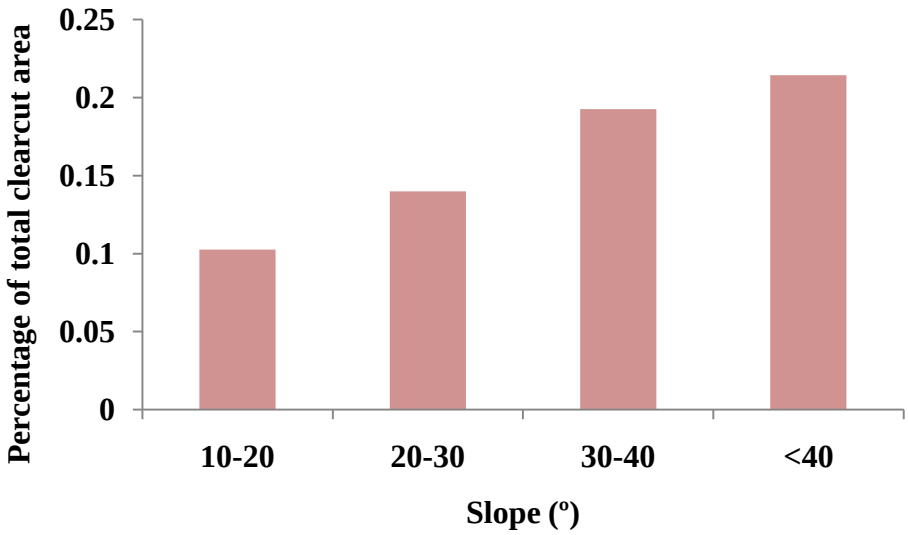

Figure 5.4 Percentage of logged area (over sub-basin 3) that experienced harvest-induced landslide activity, as a function of slope class.

To explore the sensitivity of logging-induced landslide activity under varying soil textures and pre-logging forest types, we applied a theoretical basin approach to isolate the influence of each of these factors. This involved covering the entire sub-basin with uniform soil or vegetation conditions and examining the resulting increase in landslide activity due to clear-cutting for each of the soil and vegetation classes. Figure 5.5 shows that the percentage of failed land due to harvesting in different soil classes increases as slopes become steeper, except for slopes greater than 50°. Failure percentages for slopes greater than 50° are lower than the 41-50° slopes, which is unusual for shallow landslides. This may be because landslide activity in the steepest slope class is high even under forested conditions, and therefore the logging scenario did not result in many additional landslide events. (Indeed, our model baseline (pre-harvest) simulation results for sub-basin 3 show that 0.21% and 0.63% of the areas within the 41-50° and >50° slope classes,

respectively, failed.) Comparing among the soil types, we observe that silty clay loam followed by talus and silty loam are the most susceptible soil classes to landslides. The soil properties that have the greatest influence on FS determination are soil cohesion and the angle of internal friction (Doten et al. 2006). The silty clay loom is the most vulnerable because it has both a low soil cohesion and a low angle of internal friction (Table 4.1), a combination which greatly increases the probability of landslide occurrence (Godt et al. 2008). Talus has a high susceptibility because we considered it as a loose fragmented soil with zero soil cohesion. Despite having a high cohesion and angle of internal friction, the silty clay loams are susceptible to landslides because of a poor drainage capacity. Poor drainage increases the downward weight of soil by holding much water than releasing it (Cedergren 1989). Conversely, sands have a low landslide susceptibility because of a high drainage capacity. (However, we only show sandy soil results for the lowest slope class as sand does not occur on steeper slopes. This is demonstrated by Table 5.5 which shows the area distribution with slope class for each soil type found in the Queets Basin.) Clay showed the least amount of failure. Landslides in clay soils are usually circular or deep rotational failures, which are predicted according to Bishop's method (Bishop 1955) and not represented by this model; this is why the model underestimates failure in clay soils.

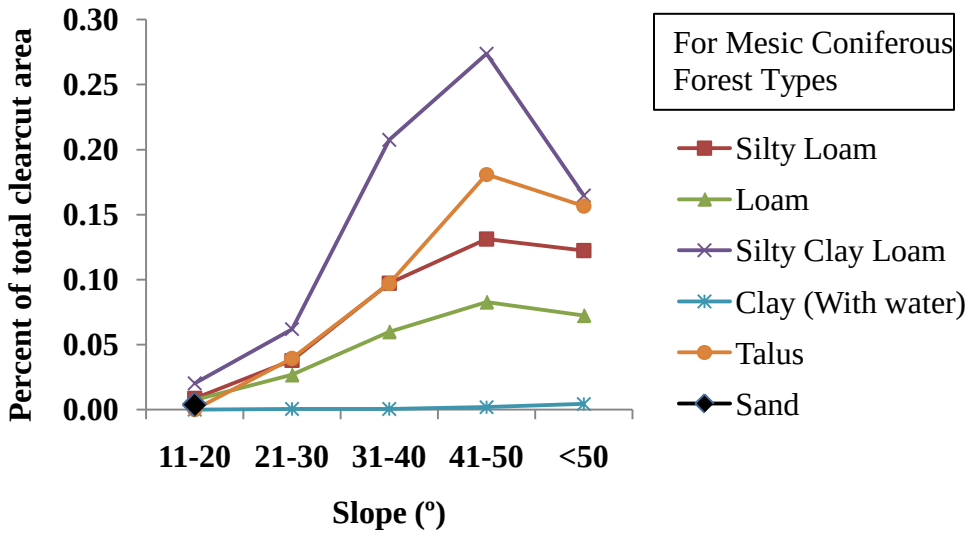

Figure 5.5 Percentage of logged area that experienced landslide activity for different soil types that have been uniformly applied over the sub-basin. A uniform pre-harvest mesic coniferous forest type was applied to isolate the effects of soils. Note: the sandy soil results are only shown for the lowest slope class because sandy soils do not occur on the steeper slopes (see Table 5.5).

Table 5.5 Soil distribution among different slope classes, expressed as a percentage.

	Slope Class (°)				
Soil Types	11-20	21-30	31-40	41-50	<50
Sand (%)	0.003	-	-	-	-
Silty Loam (%)	56.351	6.659	36.195	40.785	59.455
Loam (%)	41.648	91.915	63.303	58.926	40.150
Silty Clay Loam (%)	1.311	1.078	0.397	0.099	0.016
Clay (%)	0.563	0.304	0.093	0.172	0.354
Talus (%)	0.123	0.044	0.012	0.018	0.025

We also did a sensitivity analysis for all of the forest classes with a constant soil type (Figure 5.6). Recall from Table 4.1 that the extraction of coastal coniferous forest results in the highest amount of loss in root cohesion among all of the forest types, resulting in a high post-harvest landslide susceptibility (Sidle 1991). This behavior is observed in Figure 5.6 with post-harvest

landslide activity being highest for coastal coniferous forest, followed by mesic coniferous forest, less mature mixed forest, and deciduous broadleaf.

As with soils, harvest-induced landslide activity increases with slope steepness (except for the steepest slope class, as discussed earlier). For less steep slopes the failure percentage does not greatly differ among each of the soil and forest types; but for steeper slopes, the differences between types increase, which means some soil and vegetation types are much more resistant to failure on steep slopes than others.

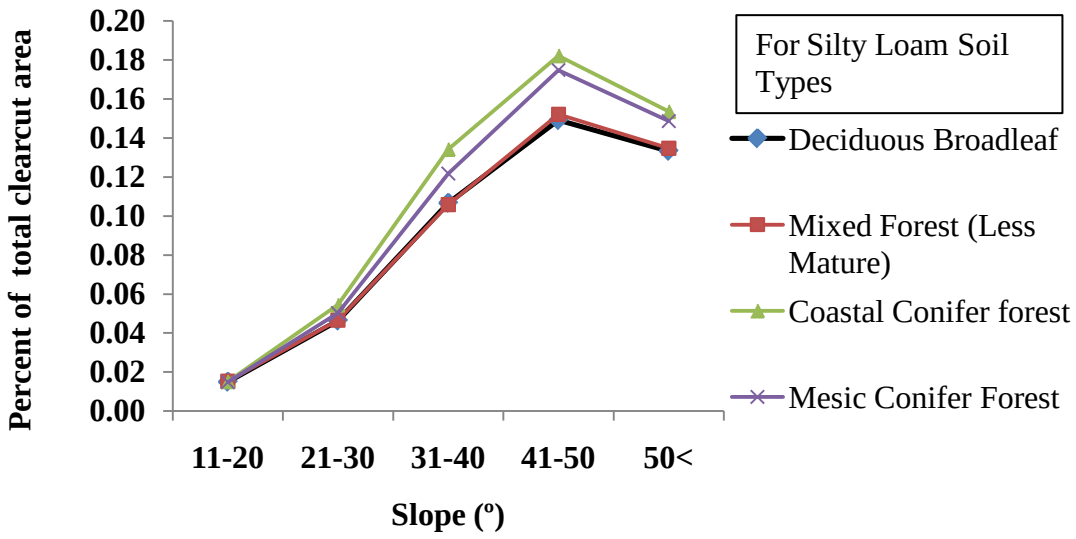

Figure 5.6 Percentage of logged area that experienced landslide activity for different pre-harvest forest types that have been uniformly applied over the sub-basin. A uniform silty loam soil type was applied to isolate the effects of vegetation.

5.5. Climate Change Effects on Logging-Induced Landslide Activity

We repeated our model simulations for the pre and post-harvest scenarios using year 2045 downscaled GCM data for each of the A1B and B1 GHG emissions scenarios. Landslide susceptibility maps over the Queets Basin were created for each of the climate change scenarios (Figure 5.7). For all of the climate change scenarios, the same landslide susceptibility thresholds (0.05 and 0.79, based on landslide susceptibility classes for historical climate) were applied to create three susceptibility classes. Table 5.7 shows the impacts of climate change on the distribution of Queets Basin pixels with susceptibility class. The number of pixels within the low susceptible class remained nearly constant but the number of pixels in the high susceptible class increased from between 3.21% to 11.07%, depending on the scenario. The highest increment (11.1%) is seen for the CNRM-CM3 model under the A1B scenario. The areas within the medium susceptibility class decreased for each of the climate change scenarios due to the transfer of cells to the highest susceptibility class. Figure 5.8 shows the new areas that moved to the high landslide susceptibility class in response to projected climate change.

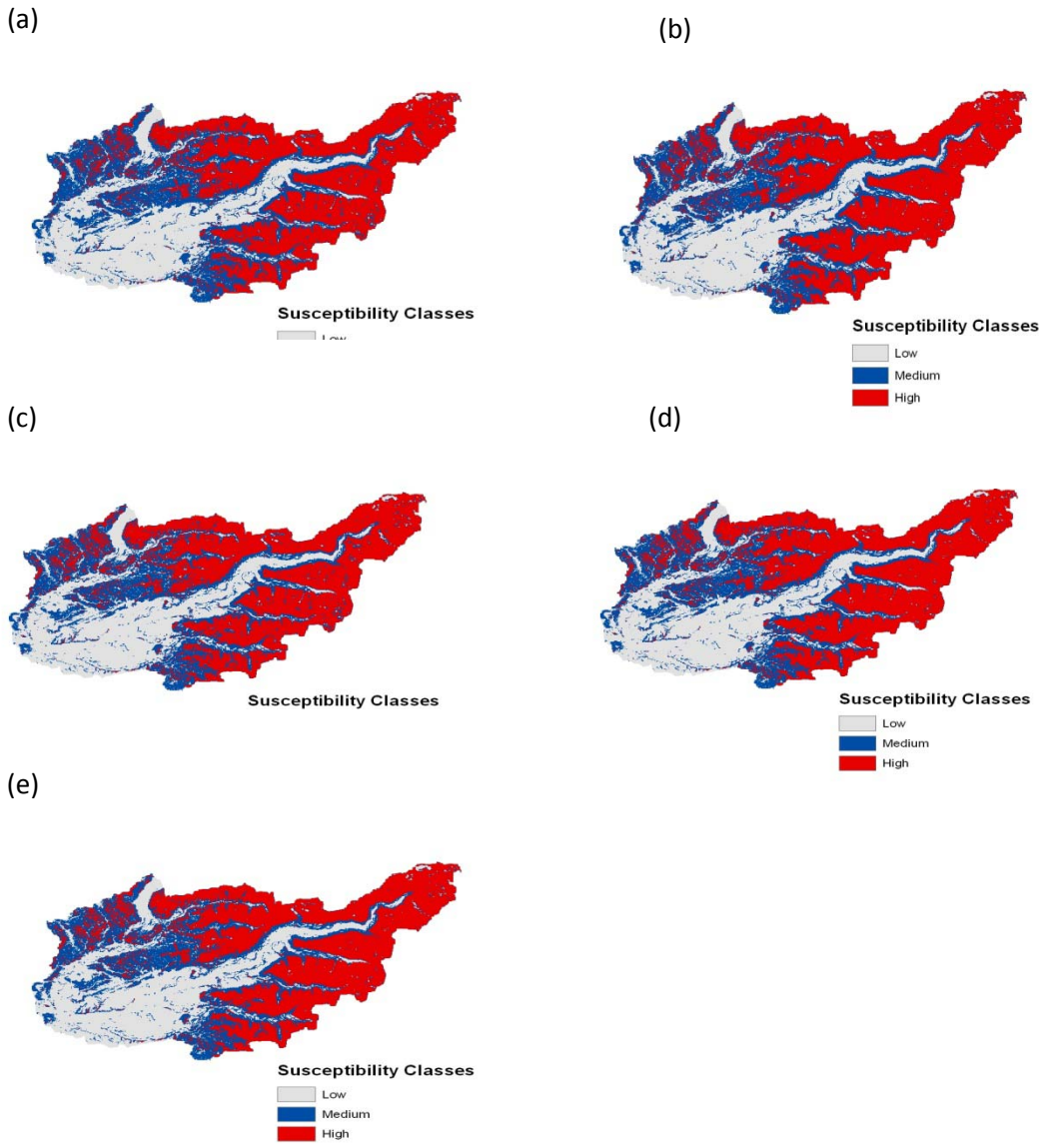

Figure 5.7 Queets Basin landslide susceptibility classes for the following climate scenarios: (a) historical, (b) CGCM_3.1t47 A1B, (c) CGCM_3.1t47 B1, (d) CNRM-cm3 A1B, and (e) CNRM-cm3 B1.

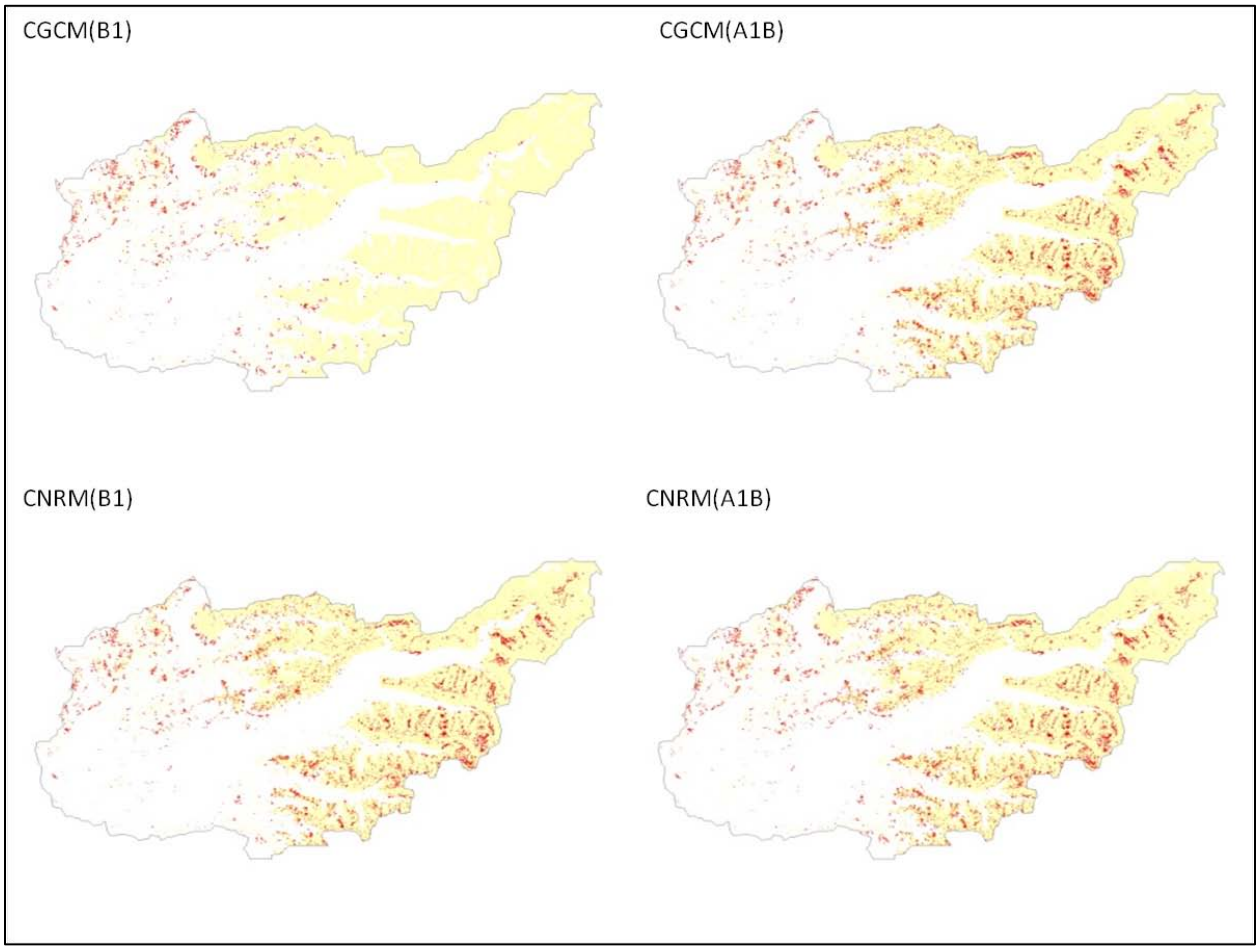

Figure 5.8 Increase in number of pixels in the high susceptibility class as a result of climate change for each climate change scenario (shown in red). The yellow pixels identify the high susceptibility areas for the historical climate scenario.

Table 5.6 Percent change in the number of 10 m resolution pixels that lie within each of the susceptibility classes with respect to the historical climate scenario.

	Number of cells in different susceptibility classes for different climate change scenarios								
Susceptibility class	Historical	CGCM_A1B	Percentage change	CGCM_B1	Percentage change	CNRM_A1B	Percentage change	CNRM_B1	Percentage change
Low	4120646	4130782	0.25	4131625	0.27	4130782	0.25	4130782	0.25
Medium	3224217	2783816	-13.66	3078979	-4.50	2750346	-14.70	2772799	-14.00
High	4187537	4617802	10.27	4321796	3.21	4651272	11.07	4628819	10.54

Chapter 6: Conclusions

Using a distributed hydrologic model (DHSVM) with a mass wasting (landslide) algorithm, we have developed a method to map logging-induced landslide susceptibility for both historical and projected year 2045 climate scenarios, with the intent that this tool may be useful to forest managers in planning for climate change. Focusing on the Queets Basin on the western slope of the Olympic Peninsula, we show that climate change will increase logging-induced landslide susceptibility (for all GCMs and GHG scenarios considered). The extent of area within the highest landslide susceptibility class increased for all climate change scenarios. Thus, for long term forest management planning, these high-risk areas should be protected from logging.

Landslide susceptibility increased on average 7.1% and 10.7% for B1 and A1B GHG emissions scenarios, respectively. Consequently, the sensitivity of landslides to climate change should be tested by isolating temperature and precipitation effects, which is something we plan to do in a subsequent sensitivity analysis. Also, the influence of snowmelt on landslides should be investigated, as increasing winter temperatures in the PNW are expected to change snowmelt patterns (Mote et al. 2003).

Results from our sensitivity simulations showed that logging-induced landslides are most sensitive in areas with steeper slopes, silty clay loam soils, and when logging in coniferous forests. For example, our baseline (pre-harvest) scenario for one of our sub-basins had a 0.008%

failure area during a single storm event; but this failure increased to as much as 0.22%, 0.27%, and 0.18%, depending on slope, soil, and pre-harvest forest types, respectively. Considering how sensitive landslide response is to variations in soil, slope, and forest types; best forest management plans should be as site-specific as possible to minimize the ecological repercussions of logging-induced landslides while ensuring the economic viability of the timber industry. For this study, we have considered the worst possible post-harvesting scenario with the lowest reduction in root cohesion. For a more rigorous study and to simulate practical management conditions, a dynamic change in root cohesion (Sidle 1991) could be incorporated into the modeling framework.

Reference List

Aellotti, P., and R. Chowdhury, 1999.Landslide hazard assessment : summery review and new perspective. Bulletin of Engineering Geology and the Environment 58(1): 28-44.

Alila, Y., and J. Beckers, 2001. Using numerical modelling to address hydrologic forest management issues in British Columbia. Hydrological Processes 15: 3371-3387.

Anbalagan, R., 1992. Landslide hazard evaluation and zonation mapping in mountainous terrain. Engineering Geology 32: 269–277.

Ayalew, L., H. Yamagishi, H. Marui, and T. Kanno, 2005. Landslides in Sado Island of Japan: Part II. GIS-based susceptibility mapping with comparisons of results from two methods and verifications. Engineering Geology 81(4): 432-445.

Beschta, R.L., 1978. Long term effect of patterns if sediment production following road construction and logging in the Oregon coast range. Water Resources Research 14(6): 1011-1016.

Bishop, A.W., 1955. The use of the slip circle in the stability analysis of slopes. Geotechnique, 5 (1): 7-17.

Blochl, A., and B. Braun, 2005. Economic assessment of landslide risks in the Swabian Alb, Germany research framework and first results of homeowners' and experts' surveys. Natural Hazards and Earth System Sciences 5: 389–396.

Brardinoni, F., M.A. Hassan, and H.O. Slaymaker, 2002. Complex mass wasting response of drainage basins to forest management in coastal British Colombia. Geomorphology 49: 109–124.

Brosofske, K.D., J. Chen, R.J. Naiman, and J.F. Franklin, 1997. Harvesting effects on microclimatic gradients from small streams to uplands in Western Washington. Ecological Applications 7(4): 1188-1200.

Brown, G.W., and J.T. Krygier, 1971. Clear-cut loggingand sediment production in the Oregon coast range. Water Resources Research 7(5): 1189-1198.

Buma, J., M. Dehn, 1998. A method for predicting the impact of climate change on slope stability. Environmental Geology 35: 2–3.

Burroughs, E. R., B. R. Thomas, 1977. Declining root strength in Douglas fir after felling as a factor in slope stability, Res. Pap. INT Intermt. For Range Exp 27: 1977.

Cedarholm, C.J., L.M. Reid, and E.O. Salo, 1981. Cumulative effects of logging road sediment on Salmonid populations in the clearwater river, Jefferson County, Washington. In: Salmon Spawning Gravel: a Renewable Resource in the Pacific Northwest Proceedings. 38–74.

Cedergren, H.R., 1989. Seepage, drainage, and flownets. John Wiley & Sons, Inc. 3rd edition.

Chander, G., and B. Markham, 2003. Revised Landsat-5 TM radiometric calibration procedures and postcalibration dynamic ranges. IEEE Transactions on Geoscience and Remote Sensing 41 (11): 2674–2677.

Chow, V.T., D.R. Maidment, and L.W. Mays, 1988. Applied Hydrology. McGraw-Hill series in water resources and engineering.

Cohen, W. B., M. Fiorella, J. Gray, E. Helmer, and K. Anderson, 1998. An efficient and accurate method for mapping forest clearcuts in the Pacific Northwest using Landsat imagery. Photogrammetric Engineering and Remote Sensing, 64: 293–300.

Collison, A., S. Wade, J. Griffiths, and M. Dehn, 2000. Modelling the impact of predicted climate change on landslide frequency and magnitude in SE England. Engineering Geology 55: 205–218.

Constantine, J.A., G.B. Pasternack, and M.L. Johnson, 2005. Logging effects on sediment flux observed in a pollen-based record of overbank deposition in a northern California catchment. Earth Surface Processes and Landforms 30: 813–821.

Dai, F.C., C.F. Lee, and Y.Y. Nagi, 2002. Landslide risk assessment and management : an overview. Engineering Geology 64: 65-87.

Daly, C., W.P. Gibson, G.H. Taylor, G.L. Johnson, and P. Pasteris, 2002. A knowledge-based approach to the statistical mapping of climate. Climate Research 22: 99–113.

Deems, J., and A.F. Hamlet, 2010. Historical Meteorological Driving Data Set. (in review).

Dhakal, A.S., and R.C. Sidle, 2003. Long-term modelling of landslides for different forest management practices. Earth Surface Processes and Landforms 28: 853–868.

Dhakal, A.S., T. Amada, and M. Aniya, 1999. Landslide hazard mapping and the application of GIS in the Kulekhani watershed, Nepal. Mountain Research and Development 19(1): 3–16.

Dixon, N., and E. Brook, 2007. Impact of predicted climate change on landslide reactivation: case study of Mam Tor, UK. Landslides 4:137–147.

DNR, 2007. Olympic Experimental State Forest: Forest land planning. Washington State Department of Natural State. OESF flp fact sheet 3-12-07.indd.

DNR, 2009. Hazard Zonation Project, landslides of Washington State at 1:24,000 scale, version 2.0. URL: http://www.dnr.wa.gov/ResearchScience/Pages/PubData.aspx (Last accessed on 1 st April 2010).

Doten, C.O., L.C. Bowling, J.S. Lanini, and E.P. Maurer, and D.P. Lettenmaier, 2006. A spatially distributed model for the dynamic prediction of sediment erosion and transport in mountainous forested watersheds, Water Resouces Research 42(4): 1-15.

Easterling, D.R., A. Gerald, G.A. Meehl, C. Parmesan, S.A. Changnon, T.R. Karl, and L.O. Mearns, 2000. Climate Extremes: Observations, Modeling, and Impacts. Science 289: 2068.

Elsner, M.M., L. Cuo, N. Voisin, A.F. Hamlet, J.S. Deems, D.P. Lettenmaier, K.E.B. Mickelson, and S.Y. Lee, 2010. Implications of 21st century climate change for the hydrology of Washington State. Climate Change (in review).

GLOVIS, 2006. USGS Global Visualization Viewer. URL: http://glovis.usgs.gov/(Last accessed on 3 rd March, 2010).

Godt, J.W., W.H. Schulz, R.L. Baum, and W.Z. Savage, 2008. Modelling rainfall conditions for shallow landsliding in Seattle, Washigton. Reviews in Engineering Geology, xx: 137-152.

Gresswell, S., D. Heller, and D. Swanston, 1979. Mass movement response to forest management in the Central Oregon Coast Range. US Department of Agriculture, Forest Service Resource Bulletin, PNW-84.

Guthrie, R.H., 2002. The effects of logging on frequency and distribution of landslides in three watersheds on Vancouver Island, British Columbia. Geomorphology 43: 273– 292.

Guzzetti, F., A.Carrara, M. Cardinali, and P. Reichenbach, 1999. Landslide hazard evaluation: a review of current techniques and their application in a multi-scale study, central Italy. Geomorphology 31: 181–216.

Hamlet, A.F., E.P. Salathe and P. Carrasco, 2010. Statistical downscaling techniques for global climate model simulations of temperature and precipitation with application to water resources planning studies (in review).

Hartman, G.F., J.C. Scrivener, and M.J. Miles, 1996. Impacts of logging in Carnation Creek, a high-energy coastal stream in British Columbia, and their implication for restoring fish habitat. Canadian Journal of Fisheries and Aquatic Sciences 53(1): 237–251.

HCDOP, 2005. Hood canal dissolved oxygen program. URL: http://www.hoodcanal.washington.edu/aboutHC/scienceprimer.jsp. (Last accessed on 3 rd March 2010).

Highland, L. M., 2003. An account of preliminary landslide damage and losses resulting from 28 February 2001, Nisqually, Washington, Earthquake. U.S. Department of the Interior and U.S. Geological Survey, Open-File Report 03-211.

Imaizumi, F., R.C. Sidle, R. Kamei, 2008. Effects of forest harvesting on the occurrence of landslides and debris flows in steep terrain of central Japan. Earth Surface Processes and Landforms 33: 827–840.

Jakob, M., 2000. The impact of logging on landslide activity at Clayoquot Sound, British Columbia. Catena 38: 279– 300.

Kalnay, E., M. Kanamitsu, R. Kistler, W. Collins, D. Deaven, L. Gandin, M. Iredell, S. Saha, G. White, J. Woollen, Y. Zhu, A. Leetmaa, R. Reynolds, M. Chelliah, W. Ebisuzaki, W.Higgins, J. Janowiak, K. C. Mo, C. Ropelewski, and J. Wang, 1996. The NCEP/NCAR 40-Year Reanalysis Project. Buletin of American Meteorological Society 77: 437-471.

Kim, S.J., G. M. Flato, G. J. Boer, and N. A. McFarlane, 2002. A coupled climate model simulation of the Last Glacial Maximum, part 1: Transient multi-decadal response. Climate.Dynamics 19, 515– 537.

Koloski, J.W., S.D. Schwarz, D.W. Tubbs, 1989. Geotechnical properties of geologic materials. Engineering Geology in Washington, Washington Division of Geology and Earth Resources Bulletin 78(1).

Lee, S., and K. Min, 2001. Statistical analysis of landslide susceptibility at Yongin, Korea. Environmental Geology 40: 1095-1113.

Lewis, J., 1998. Evaluating the Impacts of Logging Activities on Erosion and Suspended Sediment Transport in the Caspar Creek Watersheds. General Technical Report PSW-GTR-169, fs.fed.us.

Lindeburg, M.R., Civil engineering reference manual for the PE exam. Professional Publications, Incorporated. 8th Edition.

Loáiciga, H.A., D.R. Maidment, and J.B. Valdes, 2000. Climate-change impacts in a regional karst aquifer, Texas, USA. Journal of Hydrology 227: 173-194.

Lyons, J.K, and R.L. Beschta, 1983. Land use, floods and channel changes: Upper middle fork Willamette River, Oregon (1936-1980). Water Resource research 19 (2): 463-471.

Maidment, D.R. (Editor in Chief), 1992. Handbook of Hydrology. McGraw-Hill, inc.

Mantovani, F., R. Soeters, and C.J. van Westen, 1996. Remote sensing techniques for landslide studies and hazard zonation in Europe. Geomorphology 15: 213–225.

Maurer, E.P., A.W. Wood, J.C. Adam, D.P. Lettenmaier, and B. Nijssen, 2002. A long-term hydrologically-based data set of land surface fluxes and states for the conterminous United States. Journal of Climate 15: 3237-3251.

Minder, J. R., D. R. Durran, G. H. Roe, and A. M. Anders, 2008. The climatology of small-scale orographic precipitation over the Olympic Mountains: Patterns and processes. Quarterly Journal of the Royal Meteorological society 134: 817-839.

Minder, R.J., G.H. Roe, and D.R. Montgomery, 2009. Spatial patterns of rainfall and shallow landslide susceptibility. Water Resources Research 45: 1-11.

Mogami, T., 1977. Development of the mechanics of granular materials in Japan. IX ICSMFE conference, Tokyo, Japan: 42.

Montgomery, D.R., K.M. Schmidt, H.M. Greenberg, and W.E. Dietrich, 2000. Forest clearing and regional landsliding. Geology 28: 311-314.

Montgomery, D.R., K. Sullivan, and H.M. Greenberg, 1998. Regional test of a model for shallow landsliding. Hydrological Processes 12: 943-955.

Mote, P.W., and E.P. Salathé, 2010. Future climate in the Pacific Northwest. Climate Change (in review).

Mote, P.W., E.A. Parson, A.F. Hamlet, W.S. Keeton, D.P. Lettenmaier, N. Mantua, E.L. Miles, D.W. Peterson, D.L. Peterson, R. Slaughter, and A.K. Snover, 2003. Preparing for climatic change: the water, salmon, and forests of the Pacific Northwest. Climate Change 61: 45–88.

Nakićenović, N., and R. Swart (eds.), 2000. Special Report on Emissions Scenarios. A Special Report of Working Group III of the Intergovernmental Panel on Climate Change. Cambridge University Press, Cambridge, United Kingdom and New York, NY, USA, 599.

NASA, 1984. National Aeronautics and Space Administration, Landsat Program, Landsat5 TM scene SLC-Off, USGS, Sioux Falls.

NASA, 1999. National Aeronautics and Space Administration, Landsat Program, Landsat7 TM scene SLC-Off, USGS, Sioux Falls.

Nash, J.E., and J.V. Sutcliffe, 1970. River flow forecasting through conceptual models part I- A discussion of principles. Journal of Hydrology 10(3): 282-290.

NOAA, 1990. National Oceanic and Atmospheric Administration, Coastal change analysis program regional land cover. NOAA Coastal Services Center. URL: http://www.csc.noaa.gov/digitalcoast/data/ccapregional/ (Last accessed on 4th April 2010).

NOAA, 1978. National Oceanic and Atmospheric Administration, Climate of Washington. Climatography of the United States No. 60, Washington, DC.

O'Loughlin, C., 1974. The effect of timber removal on the stability of forest soils. Journal of Hydrology 13(2): 121-134.

Reeves, G.H., F. H. Everest, and J. R. Sedell, 1993. Diversity of juvenile anadromous salmonid assemblages in coastal Oregon basins with different levels of timber harvest. Transactions of the American Fisheries Society 122: 309–317.

Remondo, J., J. Bonachea, and A. Cendrero, 2008. Quantitative landslide risk assessment and mapping on the basis of recent occurrences, Geomorphology 94: 496–507.

Roering, J.J., K.M. Schmidt, J.D. Stock, W.E. Dietrich, and D.R. Montgomery, 2003. Shallow land sliding, root reinforcement, and the spatial distribution of trees in the Oregon Coast Range. Canadian Geotech Journal 40: 237–253.

Sader, S.A., and J.C. Winne 1992. RGB-NDVI colour composites for visualizing forest change dynamics. International Journal of remote Sensing, 13: 3055-3067.

Saha, A.K., R.P. Gupta, I. Sarkar, M.K. Arora, and E. Csaplovics, 2005. An approach for GIS-based statistical landslide susceptibility zonation—with a case study in the Himalayas. Landslides 2: 61–69.

Salas-M_elia, D., F. Chauvin, M. Deque, H. Douville, J. F. Gueremy, and co-authors, 2005. Description and validation of the CNRM-CM3 global coupled model. Centre National de Recherches Meteorologiques, Meteo-France, France. CNRM working note 103, 36 pp.

Schmidt, K. M., J. J. Roering, J. J. Stock, W. E. Dietrich, D. R. Montgomery, and Schaub T., 2001. Root cohesion variability and shallow landslide susceptibility in the Oregon Coast Range. Canadian Geotechnical Journal 38: 995–1024.

Schmidt, M., T. Glade, 2003. Linking global circulation model outputs to regional geomorphic models: a case study of landslide activity in New Zealand. Cliamate Research 25: 135–150.

Sidle, R.C., 1991. A Conceptual Model of Changes in Root Cohesion in Response to Vegetation Management. Journal of Environmental Quality 20:43-55.

Sidle, R.C., 1992. A theoretical model of the effects of timber harvesting on slope stability. Water Resources Reaearch 28(7): 1897-1910.

Simon, A., A.J.C. Collison, 2002. Quantifying the mechanical and hydrologic effects of riparian vegetation on streambank stability. Earth Surface Processes and Landforms 27(5): 527-546.

Skole, D., and C. Tucker, 1993. Tropical deforestation and habitat fragmentation in the Amazon: Satellite data from 1978 to 1988. Science 260:1905-1910.

Slaughter, S.L., and W. S. Jr. Lingley, 2006. Mass wasting assessment for the state lands Queets block: parts of Lower Queets River and Metheney Creek watershed administrative units, Jefferson and Grays Harbor counties, Washington. State lands landslides hazard block mapping project report. Department of Natural Resources: Land management division, Olympia, Washington.

Smith, D.W., E.E. Prepas, G. Putz, J.M. Burke, W.L. Meyer, I. Whitson, 2003. The forest watershed and riparian disturbance study: a multi-discipline initiative to evaluate and manage watershed disturbance on the Boreal Plain of Canada. Journal of Environmental Engineering and Science 2: S1–S13.

Sohn, Y., and N.S. Rebello, 2002. Supervised and unsupervised spectral angle classifiers. Photogrammetric Engineering & Remote Sensing 68(12): 1271-1280.

Soil Conservation Service, 1975. Soil taxonomy: A basic system of soil classification for marking and interpreting soil surveys. Agricultural Handbook no. 436, USDA-SCS.

Spittlehouse, D.L., R.B. Stewart, 2003. Adaptation to climate change in forest management. BC Journal of Ecosystems and Management 4(1).

SRTM, 2000. Digital Elevation Model 1 arc sec Highlands Ranch, Colorado: LandInfo Worldwide Mapping.

Swanson, F.J., and C. T. Dyrness, 1975. Impact of clear-cutting and road construction on soil erosion by landslides in the western Cascade Range, Oregon. Geology 3(7): 393-396.

Tang, S.M., J.F. Franklin, D.R. Montgomery, 1997. Forest harvest patterns and landscape disturbance processes. Landscape Ecology 12: 349–363.

U.S. Geological Survey, 1991, The National Aerial Photography Program (NAPP), [brochure]: Reston, Virginia, U.S. Geological Survey 2.

U.S. Geological Survey, 1992. The National Map. URL: http://topomaps.usgs.gov/(Last accessed on 12 th April 2010.)

U.S. Geological Survey, 2000. Shuttle Radar Topography Mission 1 arc second digital elevation data. URL: http://edcsns17.cr.usgs.gov/EarthExplorer/(Last accessed on 12 th April 2010.)

U.S. Geological Survey, 2008. Landslides Hazards Program. URL: http://landslides.usgs.gov/ (Last accessed on 7 th march 2010.)

UWESS, 2000. University of Washington Earth and Space Sciences Washington 10 m DEM. URL: http://gis.ess.washington.edu/data/raster/tenmeter/byquad/index.html (Last accessed on 12 April, 2010.)

Van Asch, T.W.J, J. Buma, and L.P.H. Van Beek, 1999. A view on some hydrological triggering systems in landslides. Geomorphology 30: 25–32.

Van Beek, L.P.H., 2002. Assessment of the Influence of Changes in Land-Use and Climate on Landslide Activity in a Mediterranean Environment. Netherlands Geographical Studies 294: 363.

Van Beek, L.P.H., and W. J. Van Asch, 2004. Regional assessment of the effects of land-use change on landslide hazard by means of physically based modeling. Natural Hazards 31: 289–304.

Van Westen, C.J., 1997. Statistical landslide hazard analysis. In: Application guide, ILWIS 2.1 for Windows. ITC, Enschede, The Netherlands 73–84.

WADNR, 2003. Soil survey data. URL: http://fortress.wa.gov/dnr/app1/dataweb/dmmatrix.html#Soils (Last accessed on 21st March 2010).

Wang H.B., and K. Sassa, 2005. Comparative evaluation of landslide susceptibility in Minamata area, Japan. Environmental Geology 47(7): 956–966.

Washington Atlas and Gazetteer, 1998. Delorme publication. 4th Edition.

Watson, A., C. Phillips, and M. Marden, 1999. Root strength, growth, and rates of decay: root reinforcement changes of two tree species and their contribution to slope stability. Plant and Soil 217: 39–47.

Wigmosta, M.S., L.W. Vail, and D. P. Lettenmaier, 1994. A distributed hydrology-vegetation model for complex terrain, Water Resources Research. 30:1665– 1669.

Wigmosta, M.S., and Lettenmaier D.P. 1999. A Comparison of Simplified Methods for Routing Topographically-Driven Subsurface Flow. Water Resources Research 35: 255-264.

Wilson, E.H., S.A. Sader, 2002. Detection of forest harvest type using multiple dates of Landsat TM imagery. Remote Sensing of Environment 80: 385– 396.

Wood, A.W., E.P. Maurer, A.Kumar, and D.P. Lettenmaier, 2002. Long range experimental hydrologic forecasting for the eastern U.S. Journal of Geophysics Research 107(D20): 4429.

Wood, A.W., L.R. Leung, V. Sridhar, and D.P. Lettenmaier, 2004. Hydrologic implications of dynamical and statistical approaches to downscaling climate model outputs. Climatic Change 62 (1-3): 189-216

Wu, W., and R.C. Sidle, 1995. A distributed slope stability model for steep forested basins. Water Resources Research 31(8): 2097-2110.

Yin, K.L., and T.Z. Yan, 1988. Statistical prediction model for slope instability of metamorphosed rocks. In: Proceedings of 5th Int Symp on Landslides, Lausanne, Switzerland 2:1269–1272.

Ziemer, R.R., J. Lewis, R.M. Rice, and T. E. Lisle, 1991. Modeling the Cumulative Watershed Effects of Forest Management Strategies. Journal of Environmental Quality 20:36-42.